Mining of Topographic Feature from Heterogeneous Imagery and Its Application to Lunar Craters

Rie Honda[1], Yuichi Iijima[2], and Osamu Konishi[1]

[1] Department of Mathematics and Information Science,
Kochi University, Akebono-cyo 2-5-1 Kochi, 780-8520, JAPAN
{honda, konishi}@is.kochi-u.ac.jp
http://www.is.kochi-u.ac.jp
[2] Institute of Space and Astronautical Science,
Yoshino-dai 3-1-1, Sagamihara Kanagawa, 229-8510, JAPAN
iijima@planeta.sci.isas.ac.jp

Abstract. In this study, a crater detection system for a large-scale image database is proposed. The original images are grouped according to spatial frequency patterns and both optimized parameter sets and noise reduction techniques used to identify candidate craters. False candidates are excluded using a self-organizing map (SOM) approach. The results show that despite the fact that a accurate classification is achievable using the proposed technique, future improvements in detection process of the system are needed.

1 Introduction

Recent advances in sensors and telemetry systems have increased the amount and quality of imagery available for researchers in fields such as astronomy, earth observation, and planetary exploration. However such advances have also increased the need for a large-scale database of scientific imagery and associated data mining techniques. [1][2][4][8][14][13].

Smyth et al.[13] and Burl et al. [1] developed a trainable software system that learns to recognize Venusian volcanos in a large set of synthetic aperture radar imagery taken by the spacecraft Magellan. A machine leaning approach was adopted because it is easier for geologists to identify feature examples rather than describe feature constraints. Experimental results showed that the system was able to successfully identify volcanos in similar imagery but performance deteriorated when significantly different scenes were used. Burl et al. also proposed an automated feature detection system for planetary imagery named Diamond Eye[2] which was applied to crater detection and showed a good performance, however, a difficulty similar with the previous study was expected.

Hamada et al.[6] reported on the automated construction of image processing techniques based on misclassification rate and an expert system composed of a large set of image processing modules.

In this paper, attention is focused on two difficulties in feature detection in optically observed image databases. The first is heterogeneity of image quality due to differences in illumination and surface conditions that affect the parameters included in the detection process. The second is the wide range of target feature sizes. For example, the diameter of lunar craters ranges from 1000 km to just 100 m (approximately equal to the size of several pixels in the object space).

A feature detection system for a large database of scientific imagery is proposed particularly focusing on detecting features with a wide range of sizes from large scale imagery of various quality at the best performance. The technique is applied to the detection of craters in lunar optical imagery.

2 System Overview

Craters are hollow features of varying size and shape and are frequently observed on solid planetary surfaces. Most craters were formed as a result of meteoroid impact. Their number and size distributions provide significant information about meteoroid activity in the past, the age and rheological properties of the planetary surface. Crater analysis has relied on human visual interpretation because of the difficulties in implementing efficient and accurate automation techniques.

In optical imagery, craters are generally recognized by shadows around the rim and represented according to the illumination conditions. Furthermore, image quality varies due to albedo, surface roughness, and illumination conditions, which further complicates the detection process.

Considering these difficulties, the following detection process is proposed: edge detection filtering, binarization, and circular pattern detection using Hough transforms or a genetic algorithm (GA). Concentrating on edge patterns reduces difficulties caused by changing illumination conditions. However, additional parameters such as the binarization threshold are introduced into the detection process and optimization of these parameters should be considered.

Thus the proposed crater detection system is descried as follows.

1. Clustering of original images.
2. Selection of representative image for each cluster and generation of teacher images by manually extracting features.
3. Optimization of detection process for each representative image by comparison with the result of 2.
4. Learning of candidate pattern for solution screening.
5. Detection of feature candidates and screening of unknown images using information obtained in 1 - 4.
6. Storage of extracted feature information in secondary database.
7. High level spatial pattern mining.

A schematic overview of processes 1 to 5 is shown is Figure 1. In this study, processes 1, 2, 3 and 4 are examined in detail and the effectiveness of integrated process evaluated by application to new imagery.

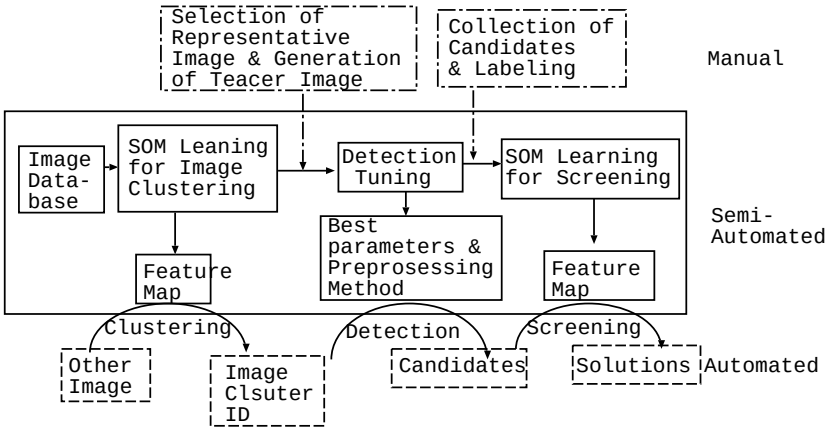

Fig. 1. System overview.

3 Candidate Detection

3.1 Crater Detection Method

In this section, the use of Hough transforms and genetic algorithm is shown as possible crater detection modules. The details of these techniques are described in the following.

Combinational Hough Transform Hough transforms are used for the extraction of geometrically simple parametric figures from binary images[10]. For crater detection, the target parameters are the center and the radius of the crater rim. Firstly, the parameter space is divided into cells (bins). Probable parameter values (or trace) are calculated for each signal (white pixel) in a binary image assuming that the signal is a part of the figure, and the count of the corresponding cell is increased by one. After all signals are counted in the parameter space, parameter sets of the figures that exist in the binary image are obtained by extracting parameter cells whose count number exceeds a threshold.

Watanabe and Shibata [15] proposed combinational Hough Transform (CHT) that uses a pair of signals in a restricted region and multiresolution images to simplify projection into a parameter space. The results showed the use of a CHT reduced computation time and significantly improved the solution accuracy. Therefore, a CHT with additional noise reduction and other minor processes to improve accuracy is proposed for crater detection[9].

The algorithm of crater detection based on CHT are summarized as follows.

1. The original binary image are preprocessed by using some of the following methods: isolated noise reduction, expansion and shrinking, thinning by Hilditch's algorithm, pyramid-like signal reduction.
2. The image is degraded using the $W \times W$ pixel filter matrix.

3. The image is divided into the $L \times L$ pixels blocks.
4. The radius of the target circle is set to be $r = L/4$. The following process from 5 to 8 are proceeded increasing r by 1 while $r \leq L/2$.
5. The processes of 6 and 7 are performed for all blocks.
6. Among pairs of white pixels in the block extended by 50% ($2L \times 2L$ pixels), $P_{i1} = (x_{i1}, y_{i1})$ and $P_{i2} = (x_{i2}, y_{i2})$, the pairs that satisfy $r \leq |P_{i1}P_{i2}| < 2r$ are selected as signal candidates.
7. The center of the circle (x_{ic}, y_{ic}) is calculated for each pair assuming they exist on a circle rim with radius of r.
8. The count of the (x_{ic}, y_{ic}, r) cell in the parameter space is increased by 1.
9. The cells are sorted concerned with number of count. If the count is larger than 0, a circle of (x_{ic}, y_{ic}, r) is projected on the image, and the normalized count and the matching ratio are calculated. The definition of both values are given by

$$NC = count(x, y, r)/np^2, \tag{1}$$

$$M = np_w/np, \tag{2}$$

where NC is the normalized count, $count(x, y, r)$ is the count of the cell (x, y, r), np is the number of pixels on the rim of projected circle, M is the matching ratio, np_w is the number of white pixels of the rim of projected circle.
Furthermore, to exclude the false solutions caused by random noises, the internal noise ratio IN within the circle with the radius of hr is introduced, where $0 < h < 1$ (typically $h = 0.6$).
10. The cells satisfying $(NC > NC_{th}) \cap (M > M_{th}) \cap (IN < IN_{th})$ are extracted as the solutions, where NC_{th}, M_{th} and IN_{th} are the thresholds for NC, M, and IN, respectively.

Since the radius of circle is restricted by L, we utilize the multiresolution image of the original grayscale image to detect the circle with the radius larger than $L/2$. It should be noted that appropriate three threshold values and noise reduction methods must be chosen to optimize the performance.

Genetic Algorithm Genetic algorithms are frequently used to obtain a single solution in optimization problems[5]. In order to implement such an algorithm for circular object detection, based on [12], a gene is set as a binary string that sequentially expresses a parameter set of (x_i, y_i, r_i), where (x_i, y_i) and r_i are the center and radius of the circle represented by the i-th gene, respectively. The fitness of the i-th gene, g_i, is calculated by projecting the circle represented by the i-th gene onto the binary image and checking its overlapping ratio, $g_i = n_i/N_i$, where n_i is the number of white pixels on the circle and N_i is the total number of pixels on the circle. In order to avoid random noise being incorporated into the solution, we modified g_i as follows:

$$g_i' = g_i - g_{i,r=fr_i}, \tag{3}$$

where $g_{i,r=fr_i}$ is the ratio of the white pixels on a circle with a radius of fr_i and $0 < f < 1.0$ (typically $f = 0.3$).

A variety of genes are then randomly produced and evolved through selection, crossing, and mutation. After iteration, genes with a fitness higher than the threshold are extracted as solutions.

Since it is possible to have many solutions (craters) in a single image, a process to unify similar genes and delete detected circles from the original images is introduced to improve the system's ability to detect multiple solutions[9]. After removal of solution circles, genes are newly generated and the process is iterated.

The algorithm of crater detection by GA is summarized as follows.

1. The original image is degraded using $W \times W$ pixel filter matrix.
2. Initial populations of genes are generated.
3. The following process from 4 to 6 are iterated for a given number of generations.
4. The fitness of genes, g'_i, are calculated.
5. The genes are selected, crossed, and mutated.
6. The genes with the same attributes are unified.
7. The genes with $g'_i > g'_{th}$ are detected as solutions, where g'_{th} is the threshold of g'.
8. The solutions are projected as circle rims on the image. The intensity of pixels on the projected circle rims are changed to 0 (black).
9. The processes from 2 to 8 are iterated for a given number of times.

The proposed algorithm also includes several parameters (e. g. g'_{th} or mutation rate) that affect solution accuracy and optimization of these parameters is dependent on image quality.

3.2 Optimization of the Detection Process

Preliminary results of tests using the above method have indicate that noise and signal gaps have a significant deterioration effect on detection accuracy[9]. The optimization of parameters such as the binarization or count threshold is effective technique for improving accuracy, however, the optimized values are dependent on image quality.

The following optimization process is suggested: (1) cluster source images, (2) select representative image from each group, (3) produce teacher image by manual visual recognition, (4) optimize crater detection process by comparing results from teacher images and the result from the corresponding original image. The details of these sub-processes are provided in the following section.

Clustering of Frame Images It is suggested that the rough grouping of images with respect to image quality is an effective technique for simplifying optimization of the detection process. In this study, the clustering of original images using Kohonen's self-organizing maps (SOM) [11] was examined.

SOM is an unsupervised learning algorithm that uses a two-layer network of input layer and competition layers, both of which are composed of units with n-th dimensional vectors. SOM effectively maps the similar pattern of the input layer on the competitive layer. In the SOM algorithm, the distance (usually Euclidean) between the input vector and each unit vector of the competition layer is calculated and the input vector is placed into the winner unit, which has

the smallest distance. At the same time, the unit vectors in the cells adjacent to the winner cell (defined by the neighborhood distance) are modified so that they move closer to the input vector. As a result of this iterative projection and learning, the competitive layer learns to reflect variation of the input vectors and can obtain adequate clustering of the input vectors. Presently, SOM is widely used for the clustering, visualization and abstraction of unknown data sets.

Selection and preprocessing of input vectors is crucial to improve SOM accuracy. In order to group lunar images according to roughness or contrast, the FFT power spectrum of normalized images is adopted as the input vector.

After clustering, a representative image, which has the largest similarity with the unit vector and also includes many craters, is selected for each unit cell (cluster). Then craters are marked in each representative image and binary teacher images generated (see Figure 2(a) and 2(b)).

Method of Optimization The detection process is divided into three parts for optimization purposes: binarization, preprocessing including noise reduction, and circle detection. These processes are optimized sequentially using teacher images.

Firstly, edge detection filtering is carried out on the original images. Then, optimal binarization threshold that produce a binary image most similar to the teacher image is identified for each cluster. Based on [6], the evaluation function is defined by

$$\begin{aligned} E_k = \quad & P(T_k(i,j) = S_k(i,j) \mid T_k(i,j) = 1) \\ & -\alpha P(T_k(i,j) \neq S_k(i,j) \mid T_k(i,j) = 0), \end{aligned} \tag{4}$$

where k is the cluster ID, $T_k(i,j)$ is the intensity of the (i,j) pixel of teacher binary image, α is a weight parameter (typically $\alpha = 0.3$), and $S_k(i,j)$ is the intensity of (i,j) pixel of the final binary image defined by

$$S_k(i,j) = \begin{cases} 1 & \text{for } Q_k(i,j) > Q_{th,k} \\ 0 & \text{for } Q_k(i,j) \leq Q_{th,k}, \end{cases} \tag{5}$$

where $Q_k(i,j)$ is image intensity after edge detection filtering and $Q_{th,k}$ is the binarization threshold. The value of $Q_{th,k}$ is searched greedily to maximize E_k.

Next the combination of preprocessing methods that maximizes true positive detection rate (ratio of detected true solutions to all possible true solutions) of craters defined by $Pr_k = N_k/Nt_k$ is identified, where N_k and Nt_k are the numbers of craters detected from the binary image and the teacher binary image for cluster k, respectively.

Finally, the circle detection parameters that maximize Pr_k for the preprocessed image using selected methods is identified. Figure 2 shows a schematic view of the optimization process.

As shown in Figure 2(d), extracted solutions may include many false solutions, which will be excluded in the post-processing stage described in the following section.

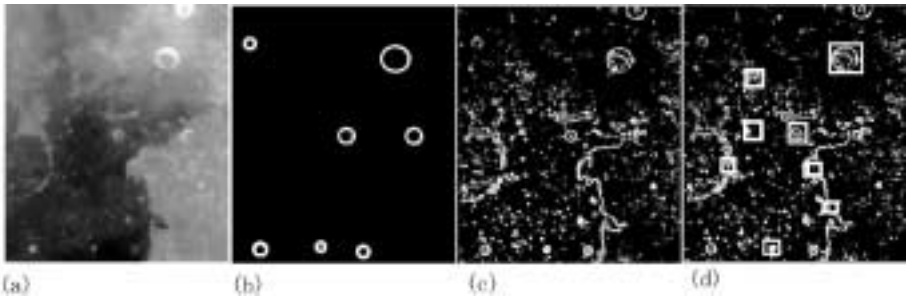

Fig. 2. Schematic view of optimization process. (a), (b), (c), and (d) show the original image, teacher image, tuned binary image, and results of detection, respectively. White squares in (d) indicate the extracted candidates.

3.3 Screening of Solutions

A solution screening process is used in the post-processing stage to exclude false solutions. Candidate crater images are cut out, normalized with respect to its size and intensity, and visually labeled true or false. The candidate pattern is learned by SOM taking the normalized intensity vectors or FFT power spectrum as the input vectors. Each unit in the competition layer is labeled either true or false by evaluating the ratio of candidates in it. If we assume that the properties of the new data set are similar to those of the studied data set, the class (true or false) of the newly detected candidate is decided by projecting it onto the SOM feature map.

4 Experiments

4.1 Description of Data Set

A total of 984 medium browse images from Lunar Digital Image Model (LDIM), which had been mosaiced by the U. S. Geological Survey based on the lunar global images obtained by the U. S. Clementine spacecraft. The images were between 322 and 510 pixels in width and 480 pixels in height, and resampled at a space resolution of approximately 500 m/pixel using a sinusoidal projection. Images in the polar regions were not used to avoid distortions due to the map projection. The radius of target craters ranged from 2 to 18 pixels.

For clustering of original images, an area of 256×256 pixels was extracted from the center of the normalized images, and the FFT power spectrum calculated as the input vectors of the SOM. The size of the SOM competition layer was defined as 4×4 units because only a rough grouping was needed. One hundred images were sampled and the SOM leaning process iterated 100000 times. All images were then projected onto the competition layer, and the unit cell vectors adjusted using K-means method[3]. No images with extremely large distance were identified in this process.

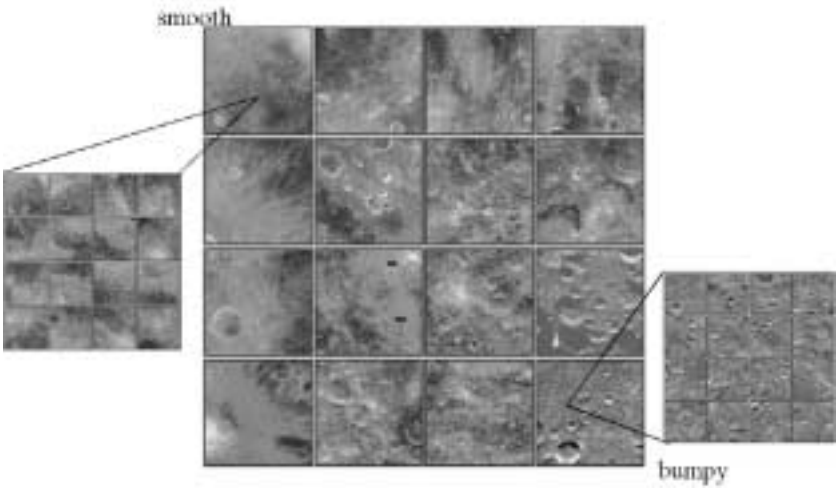

Fig. 3. SOM feature map for clustering of original images. Cluster ID 0, 1, 2, . . . , and 15 are for each cell from the upper left corner to the lower right corner in raster-scan order.

4.2 Result of Image Clustering

Figure 3 shows the resulting competition layer, hereafter denoted the feature map. In this map, the image with the smallest distance with each unit vector is displayed in each cell to visualize the clustering result. It can be seen that relatively smooth images including the Mare recognized by a dark region, are clustered on the left side, and the rugged terrains called the Highland with many clearly identifiable craters are clustered in the lower right corner. This result indicates that learning by SOM successfully distinguishes between variations in image quality and groups them effectively. Based on the clustering result, a representative image was manually selected and a teacher binary image produced for each cluster.

4.3 Result of Detection Optimization

Table 1 shows an example of optimized parameters for CHT case, in which the result of noise reduction method are common to both CHT and GA.

The binarization threshold ranged from 30 to 125 and binary images that approximated the teacher images were produced automatically. It is suggested that a single threshold value for the entire image will not be adequate in some cases because of spatial variations within the image, and that this problem should be solved at the pre-processing stage.

For the optimization of the noise reduction processes, 12 combinations of four noise reduction methods was examined: thinning by Hilditch's algorithm[7], pyramid-like signal reduction, isolated noise reduction, and expansion and shrinking. Result of experiments showed that combination of thinning and isolated

Table 1. Teacher Image list together with optimized parameters for CHT case. Abbreviations TH, PY, IS and ES represent thinning by Hilditch's algorithm[7], pyramid-like signal reduction, isolated noise reduction, and expansion and shrinking, respectively.

ClusterID	ImageID	No. of target crater	Q_{th}	Noise reduction method	NC_{th}	M_{th}	IN_{th}
0	bi03n051	9	30	IS+TH	0.55	0.30	0.47
1	bi10n093	10	70	IS+TH	0.45	0.20	0.47
2	bi45n065	11	50	TH+PY	0.55	0.25	0.80
3	bi31n063	12	55	IS+TH	0.55	0.60	0.47
4	bi17n039	6	25	TH+PY	0.55	0.60	0.80
5	bi38s335	35	55	ES	0.45	0.45	0.80
6	bi17s225	19	85	IS+TH	0.45	0.60	0.80
7	bi38s045	44	95	IS+TH	0.35	0.60	0.80
8	bi17s027	12	95	IS+TH	0.55	0.60	0.47
9	bi03n285	15	85	IS+TH	0.45	0.50	0.80
10	bi31s039	20	125	IS+TH	0.55	0.40	0.47
11	bi80s015	36	70	IS+PY	0.45	0.20	0.80
12	bi03s039	10	80	IS+TH	0.55	0.20	0.80
13	bi38s155	13	90	IS+TH	0.55	0.35	0.30
14	bi45s335	22	105	IS+TH	0.45	0.25	0.80
15	bi59s052	59	95	IS+TH	0.35	0.20	0.30

noise reduction scored the highest positive solution detection rate for most cases (12 cases in 16). Thus we applied combination of thinning and isolated noise reduction to images of all clusters in the following process for simplicity.

Figure 4 summarizes the results of the optimization of the detection process for both CHT and GA techniques as performance curves represented by true positive detection rate as functions of the false solution number. In general, a decrease in threshold leads to an increase in both the true positive detection rate and the number of false solutions. Figure 4 shows that true positive detection rate increases with number of false solutions when the number of false solutions is relatively small, however, it remains constant for lager numbers. Thus the initial point of the flat portion of the performance curve is considered to be the optimum performance condition. In most cases, this coincides with the point that minimizes the false number and maximizes the positive rate.

Figure 4 also shows that CHT performs significantly better than GA. This is mainly caused by the fact that GA's are used to obtain a single solution. Although the GA was modified to obtain multiple solutions, the results show that the GA can acquire only a few solutions per trial even for teacher binary images that include clearly identifiable circles, and requires many iterations to acquire multiple solutions. Thus, CHT was selected as the circle detection module suitable for crater detection.

After optimization, the CHT positive solution detection rate increased significantly up to values ranging from 0.2 to 0.6. However, since information was lost

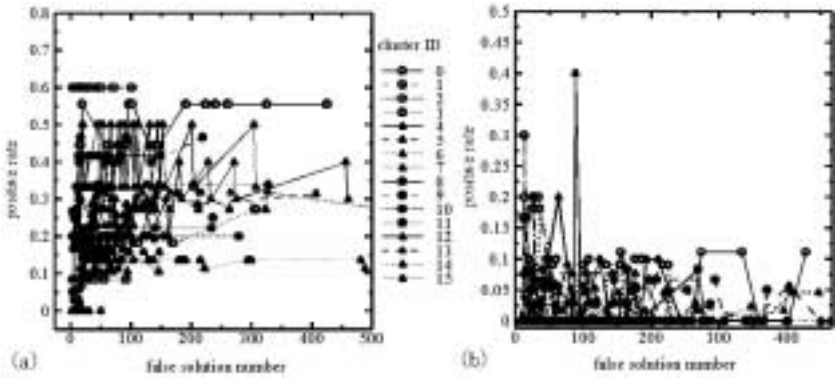

Fig. 4. Optimization result for CHT(a) and GA(b).

during the binarization process, it will be necessary to consider other detection methods for some clusters to further improve detection performance.

4.4 Result of Screening of Detected Candidates

SOM clustering of crater candidates extracted in the previous process was performed for screening purposes to produce the candidate classifier. A total of 646 candidates were visually labeled either true or false. Half of the candidates were randomly sampled for learning and the remainder were used for examination purpose. The percentage of true candidates for both groups was 25.4% and 27.2%, respectively. All images were rotated such that the direction of sunlight incidence was equal, and normalized with respect to intensity and size. Two types of input vectors were examined: image vectors represented by pixel intensities aligned in a raster-scan order, and the FFT power spectrum. The size of the SOM competition layer was set to 6×6 units by trial and error and 323000 iteration were performed. The neighborhood distance at iteration t is given by $2(1 - t/323000)$.

Figure 5 shows an example feature map obtained after SOM learning. Cells enclosed by thick frames contain more than 50% true solutions and hence were labeled true candidate cells. The remainder are labeled false cells. Figure 5 shows a cluster of true candidate cells in the upper right corner. To examine SOM classification ability, the precisions for true cells and false cells (ratio of actual true solutions to the solutions predicted true and vice versa), and accuracy (ratio of solutions predicted correctly to all data) were calculated from 5 trials.

Table 2 summarizes the results of both learning from the study data and clustering for the test data using the map with the best precision for true. The result shows that learning using image vectors was more accurate than that using the FFT power spectrum and classified candidates with an accuracy of 89.7%, which is much higher compared with the value of 78.4% for FFT power spectrum.

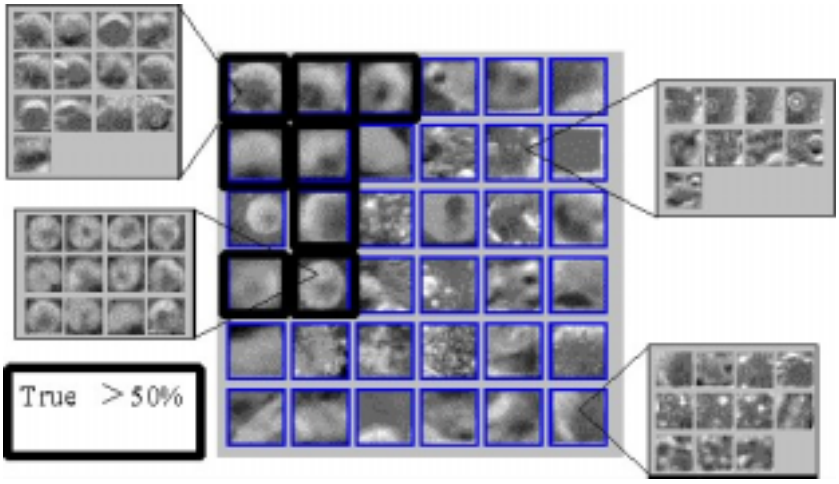

Fig. 5. Example of SOM feature map for classification of crater candidates. Input vectors are set to be image vectors.

Table 2. Result of SOM learning for crater candidate screening.

Input data	Case	Precision(true)	Precision(false)	Accuracy
Image Vector	study	0.812±0.037	0.931±0.009	0.897±0.016
	best/study	0.855	0.946	0.929
	test	0.776	0.891	0.864
FFT power spectrum	study	0.691±0.037	0.803±0.096	0.784±0.013
	best/study	0.733	0.788	0.783
	test	0.605	0.768	0.755

The most accurate map classified the unknown data with an accuracy of 86%. This indicates that the utilization of SOM feature map learned from image vectors is an effective technique for the classification of solution candidates. It should also be noted that selecting the most suitable map from the trials is important to improve classification accuracy because performance varied significantly according to the initial conditions.

5 Application to Other Imagery

The effectiveness of the proposed technique for crater detection was examined using imagery that had not been used in the optimization process. In addition, multiresolution images were used to handle craters with a wide range of sizes. By setting the radius of target crater ranging from 9 to 18 pixels, it was possible to detect craters with a radius up to 72 pixels using the multiresolution images of three levels.

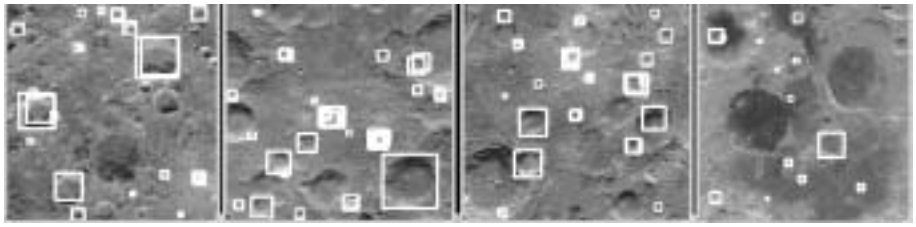

Fig. 6. Example of crater detection for other general images. The images are 480 pixels in height.

Figure 6 shows examples of detection and screening results for four images. It can be seen that detection ability is improved significantly even without manual operations. Unfortunately, the achieved detection rate is not for scientific analysis (e. g. detection rate required to be much more than 60%), thus other detection methods should be considered for some groups and the selection of circle detection modules should also be included in future work. However, our methods is considered to be sufficient for some applications such as autonomous spacecraft tracking in that high precision and moderate detection rate are required.

6 Conclusions

A technique for mining features from sets of large scale of optical imagery of various quality has been proposed. The original images were grouped according to spatial frequency patterns, and optimized parameter sets and noise reduction methods were used in the detection process. Furthermore, to improve solution accuracy, false solutions were excluded using SOM feature map that learned true and false solution patterns from a large number of crater candidates. Application of the extracted information to new imagery verified effectiveness of this approach.

The detection rate achieved in this study, however, is not sufficient in comparison with the requirements for scientific analysis and it is necessary to include other detection methods in the future work. However, we believe combining automated abstraction and summarization processes with the accurate manual techniques is crucial for the development of an accurate scientific data mining system. The proposed technique is applicable to various applications in which specific features need to be extracted from large-scale of imagery databases.

7 Acknowledgements.

The authors are grateful to Syuta Yamanaka and Hisashi Yokogawa for their past contribution amd anonymous reviewers for helpful comments. This research is supported by a grant-in-aid for intensive research (A) (1) (Project 1130215) from the Ministry of Education, Culture, Sports, Science and Technology of Japan.

References

1. Burl, M.C., Asker, L., Smyth, P., Fayyad, U.M., Perona, P., Crumpler, L., Aubele, J.: Learning to recognize volcanos on Venus. Machine Learning, **Vol. 30**, (2/3) (1998) 165–195
2. Burl, M. C. et al., Mining for Image Content, Systems, Cybernetics, and Informatics / Information Systems: Analysis and Synthesis, (Orlando, FL) (1999)
3. Duda, R. O. and Hart, P. E., Pattern Classification and Scene Analysis, John Willey and Sons, New York (1973)
4. Fayyad, U.M., Djorgovski, S.G., Weir, N.: Automatic the analysis and cataloging of sky surveys. Advances in Knowledge Discovery and Data Mining, AAAI Press/MIT Press (1996) 471–493
5. Goldberg, D. E., Genetic Algorithm in search optimization and machine learning, Addison Wesley, Reading (1989)
6. Hamada, T., Shimizu, A., Hasegawa, J., Toriwaki, J.: A Method fo Automated Construction of Image Processing Procedure Based on Misclassification Rate Condition and Vision Expert System IMPRESS-Pro (in Japanese), Transaction of Information Processing Society of Japan, **Vol. 41**, No. 7 (2000) 1937–1947
7. Hilditch, C. J. Linear skeletons from square cupboards, Machine Intelligence 4, Edinburgh Univ. Press, Edinburgh, (1969) 403-420
8. Honda. R., Takimoto, H, Konishi, O.: Semantic Indexing and Temporal Rule Discovery for Time-series Satellite Images, Proceedings of the International Workshop on Multimedia Data Mining in conjunction with ACM-SIGKDD Conference, Boston, MA (2000) 82–90
9. Honda, R., Konishi, O, Azuma, R, Yokogawa, H, Yamanaka, S, Iijima, Y : Data Mining System for Planetary Images - Crater Detection and Categorization -, Proceedings of the International Workshop on Machine Learning of Spatial Knowledge in conjunction with ICML, Stanford, CA (2000) 103–108
10. Hough, P. V. C., Method and means for recognizing complex patterns, U. S. Patent, 069654 (1962)
11. Kohonen, T.: Self-Organizing Maps, 2nd eds., Springer (1997)
12. Nagase, T. and Agui, T. and Nagahashi, H., Pattern matching of binary shapes using a genetic algorithm (in Japanese), Transaction of IEICE, **Vol. J76-D-II**, No. 3, (1993) 557-565
13. Smyth, P., Burl, M.C., Fayyad, U.M.: Modeling subjective uncertainty in image annotation. In Advances in Knowledge Discovery and Data Mining, AAAI Press/MIT Press (1996) 517–539
14. Szalay, A., Kunszt, P. Thakar, A., Gray, J. Slutz, D. and Brunner, R.J. : Designing and Mining Multi-terabyte Astronomy Archives: The Sloan Digital Sky Survey, Proceeding ACM-SIGMOD International Conference on Management of Data, Dallas TX (2000) 451–462
15. Watanabe, T. & Shibata, T., Detection of broken ellipse by the Hough transforms and Multiresolutional Images (in Japanese), Transaction of IEICE, **Vol. J83-D-2**, No. 2, (1990) 159–166